doi:10.1093/brain/awn262 Brain 2009: 132; 213–224 | 213

BRAIN
A JOURNAL OF NEUROLOGY

Graph theoretical analysis of magnetoencephalographic functional connectivity in Alzheimer's disease

C. J. Stam,[1] W. de Haan,[2] A. Daffertshofer,[3] B. F. Jones,[4] I. Manshanden,[1] A. M. van Cappellen van Walsum,[5,6] T. Montez,[7] J. P. A. Verbunt,[1,8] J. C. de Munck,[8] B. W. van Dijk,[1,8] H. W. Berendse[2] and P. Scheltens[2]

1 Department of Clinical Neurophysiology and MEG, Amsterdam, The Netherlands
2 Department of Neurology, Alzheimer Center, VU University Medical Center, Amsterdam, The Netherlands
3 Research Institute MOVE, VU University, Van der Boechorststraat 9, 1081 BT Amsterdam, The Netherlands
4 Dementia Research Centre, Institute of Neurology, UCL, London, UK
5 Department of Anatomy, Radboud University Nijmegen Medical Centre, Nijmegen, The Netherlands
6 Institute of Technical Medicine, University of Twente, Enschede, The Netherlands
7 Institute of Biophysics and Biomedical Engineering, Faculty of Sciences, University of Lisbon, Portugal
8 Department of Physics and Medical Technology, VU University Medical Center, Amsterdam, The Netherlands

Correspondence to: Willem de Haan,
Department of Neurology, Alzheimer Center,
VU University Medical Center, PO Box 7057,
1007 MB Amsterdam, the Netherlands
E-mail: w.dehaan@vumc.nl

In this study we examined changes in the large-scale structure of resting-state brain networks in patients with Alzheimer's disease compared with non-demented controls, using concepts from graph theory. Magneto-encephalograms (MEG) were recorded in 18 Alzheimer's disease patients and 18 non-demented control subjects in a no-task, eyes-closed condition. For the main frequency bands, synchronization between all pairs of MEG channels was assessed using a phase lag index (PLI, a synchronization measure insensitive to volume conduction). PLI-weighted connectivity networks were calculated, and characterized by a mean clustering coefficient and path length. Alzheimer's disease patients showed a decrease of mean PLI in the lower alpha and beta band. In the lower alpha band, the clustering coefficient and path length were both decreased in Alzheimer's disease patients. Network changes in the lower alpha band were better explained by a 'Targeted Attack' model than by a 'Random Failure' model. Thus, Alzheimer's disease patients display a loss of resting-state functional connectivity in lower alpha and beta bands even when a measure insensitive to volume conduction effects is used. Moreover, the large-scale structure of lower alpha band functional networks in Alzheimer's disease is more random. The modelling results suggest that highly connected neural network 'hubs' may be especially at risk in Alzheimer's disease.

Keywords: Alzheimer's disease; functional connectivity; MEG; synchronization; small-world networks

Abbreviations: EEG = electro-encephalography; MEG = Magneto-encephalography; MMSE = mini mental state examination; PLI = phase lag index; SL = synchronization likelihood

Received May 5, 2008. Revised September 12, 2008. Accepted September 18, 2008. Advance Access publication October 24, 2008

Introduction

A central question in cognitive neuroscience is how cognitive functions depend upon coordinated and integrated activity of specialized, widely distributed brain regions. There is strong support that a network perspective on the brain is required in order to understand higher brain functioning (Varela *et al*., 2001; Le van Quyen, 2003). How do functional interactions between brain regions take place, and how can this be measured and assessed? For answering these questions an important idea is the so-called functional connectivity that refers to linear or nonlinear statistical interdependencies between time series of physiological signals recorded from different brain regions (Aertsen *et al*., 1989; Friston, 2001; Lee *et al*., 2003; Fingelkurts *et al*., 2005). Functional connectivity is assumed to reflect functional interactions between the underlying brain regions.

The concept of functional connectivity has become very important in the study of brain mechanisms underlying disturbed cognition in Alzheimer's disease, the most frequent cause of dementia in the western population (van der Flier and Scheltens, 2005). Alzheimer's disease is characterized by degeneration of neurons starting in the hippocampus, later spreading to the temporal and parietal cortex, and finally involving most cortical areas. Loss of neurons, involvement of white matter as well as disturbed synaptic transmission, e.g. due to decreased levels of acetylcholine (Osipova *et al*., 2003), account for abnormal functional interactions between cortical regions. It has even been suggested that Alzheimer's disease can be viewed as a disconnection syndrome (Delbeuck *et al*., 2003). Support for this concept comes from a number of EEG and magneto-encephalography (MEG) studies using conventional coherence as a measure of functional connectivity (Leuchter *et al*., 1992; Besthorn *et al*., 1994; Dunkin *et al*., 1994; Jelic *et al*., 1996; Locatelli *et al*., 1998; Berendse *et al*., 2000; Knott *et al*., 2000; Stevens *et al*., 2001; Adler *et al*., 2003; Hogan *et al*., 2003; Jiang 2005; Koenig *et al*., 2005; Pogarell *et al*., 2005). In most of these studies a consistent decrease of coherence in the alpha and beta band was reported, whereas results for other bands were more variable. Abnormalities of functional connectivity have also been demonstrated with nonlinear synchronization methods (Jeong *et al*., 2001; Stam *et al*., 2002, 2006; Pijnenburg *et al*., 2004; Babiloni *et al*., 2004). While these studies in general support the hypothesis of a disconnection syndrome in Alzheimer's disease, two problems need further attention: (i) assessment of functional connectivity with EEG and MEG can be biased by volume conduction, which may yield spurious correlations between nearby sensors and hence render interpretation unreliable; (ii) connectivity studies in Alzheimer's disease are generally very descriptive and lack a more robust framework to discriminate between normal and abnormal networks in the brain.

Nearby EEG electrodes or MEG sensors are likely to pick up activity of identical sources, resulting in strong correlations between recorded signals that reflect simple volume conduction rather than true functional connectivity (Nunez *et al*., 1997; Srinivasan *et al*., 2007). Two approaches have been submitted to overcome this problem. First, one may study interdependencies between time series of reconstructed sources rather than signals of recording electrodes or sensors (Gross *et al*., 2001; David *et al*., 2002; Tass *et al*., 2003; Amor *et al*., 2005; Hadjipapas *et al*., 2005; Lehmann *et al*., 2006). While this approach has certainly the added benefit of dealing with interactions between anatomically well-defined brain regions, a major pitfall is the absence of a unique definition of the corresponding source space. Different assumptions may lead to different source models and, hence, different results. However, to date there is no reliable way to decide which model is the proper choice. Second, one may look for time series analysis techniques that extract interdependencies between signals which are not or at least unlikely due to volume conduction. This measure therefore reflects true interactions. An early attempt in this direction was summarized in a study by Nunez and colleagues (1997) who proposed to subtract a baseline random coherence from the measured coherence in order to obtain a reduced, task-related coherence, which is less influenced by volume conduction effects. More recently Nolte and colleagues (2004) proposed to use the imaginary part of the (complex-valued) coherency between two signals. Indeed volume conduction cannot give rise to imaginary coherency, but the magnitude of the imaginary part does not appear to be a proper value to quantify synchronization, since it mixes information on coupling strength and coupling delay. As an alternative, a so-called phase lag index (PLI) was introduced, which reflects the consistency with which one signal is phase leading or lagging with respect to another signal (Stam *et al*., 2007*b*). The PLI was shown to be less affected by volume conduction than more traditional measures like coherence, and by the same token, it is rather sensitive to true changes in synchronization. Here we will exploit this capacity to address possible changes in functional connectivity due to Alzheimer's disease, as we see an advantage of PLI to 'reduced coherency'. Although the latter method might represent an improvement over traditional coherence, it does rely on several a priori assumptions such as stationarity and linearity, and is still sensitive to signal amplitude. PLI is sensitive to non-linear data and can handle non-stationary data, at least to a large degree.

The theoretical framework for understanding large-scale networks is given by 'modern network theory' (for a review see Boccaletti *et al*., 2006), a branch in graph theory, in which networks are represented by a set of nodes (vertices) and connections (edges). See Fig. 1 for an explanation of the basic principles of graph theory used in this study.

In recent years, graph theory has been introduced to the study of anatomical and functional networks in the central nervous system (Bassett and Bullmore, 2006; Stam and Reijneveld, 2007*c*). Graph theory provides models of complex networks in the brain, and allows one to better understand the relations between network structure and the processes taking place on those networks. It can also provide a concept of an 'optimal' network (for example in terms of balancing segregation and integration, performance and cost), and offers scenarios of how complex networks might develop, and how they might respond to different types of damage. Watts and Strogatz (1998) introduced so-called 'small-world' networks, which have a balance between local specialization and global integration that is optimal for information processing, and they showed that several real-life networks possess small-world features. Small-world networks have

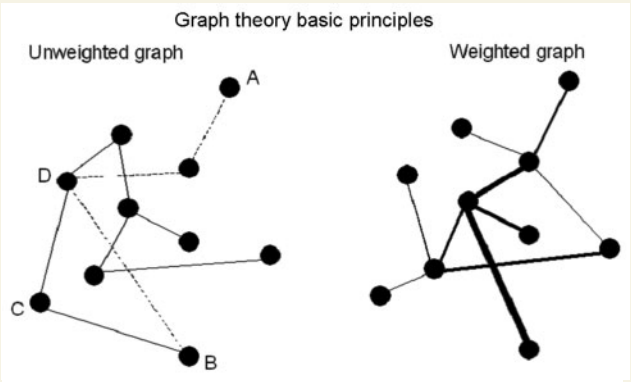

Fig. 1 Representation of a network as a graph. Black dots represent the nodes or vertices, and the lines connecting the dots the connections or edges. The left panel shows an unweighted graph. The shortest path length (L) between vertices A and B consists of three edges, indicted by the striped lines. The clustering coefficient (C) of a vertex is the likelihood that its neighbours are connected. For vertex C, with neighbours B and D, the clustering coefficient is 1. When weights are assigned to the edges, the graph is weighted (right panel). Here the weights of the edges are indicated by the thickness of the lines. Figure taken with permission from Stam and Reijneveld. Graph theoretical analysis of complex networks in the brain. *Non-linear Biomedical Physics* 2007*c*; 1: 3.

a relatively high amount of so-called 'local clustering', meaning that nodes are often connected to their neighbours, combined with relatively short 'path lengths', which means that from any node it takes just a few steps to reach any other node in the network. There is now accumulating evidence that different types of structural brain networks display a 'small-world' type network organization characterized by a combination of high local clustering as well as short path lengths (Watts and Strogatz, 1998; Hilgetag *et al*., 2000; He *et al*., 2007; Iturria-Medina *et al*., 2008). A similar approach has also been used to study networks of functional connectivity. In several fMRI studies of healthy subjects, small-world patterns were found (Salvador *et al*., 2005; Achard *et al*., 2006; Supekar *et al*., 2008). The presence of small-world type functional networks in healthy subjects was also confirmed in numerous EEG and MEG studies (Stam, 2004; Bassett *et al*., 2006; Smit *et al*., 2007; Stam *et al*., 2007*a*). However, only a few studies have yet shown that brain pathology may interfere with the normal small-world architecture. According to Bartolomei *et al*. (2006) brain networks in patients with low-grade glioma's are more random compared with healthy controls. A similar change in network structure was reported in patients with schizophrenia and in patients with epilepsy during the interictal state (Micheloyannis *et al*., 2006; Ponten *et al*., 2007; Rubinov *et al*., 2007). In a recent pilot study on Alzheimer's disease a loss of the normal small-world architecture was reported (Stam *et al*., 2006). In view of these findings one might speculate that brain disease in general gives rise to a deviation from the normal, optimal small-world configuration of brain networks. It is not clear, however, how such network changes come about.

As mentioned above two questions were addressed in the present study: (i) is it possible to confirm previous EEG and MEG reports of decreased resting state functional connectivity in Alzheimer's disease using a method that is less affected by volume conduction? (ii) can graph analysis reveal abnormalities in the large-scale topology of functional connectivity networks in Alzheimer's disease, and can such network changes be explained by modelling?

Materials and Methods

Patients and controls

Subjects and recordings were identical to Stam *et al*. (2006). The study involved 18 patients (mean age 72.1 years, SD 5.6; 11 males; mean MMSE 19.2, range: 13–25) with a diagnosis of probable Alzheimer's disease according to the NINCDS-ADRDA criteria (McKhann *et al*., 1984) and 18 healthy control subjects (mean age 69.1 years, SD 6.8; seven males; mean MMSE 29, range: 27–30), mostly spouses of the patients. Patients and controls were recruited from the Alzheimer Centre of the VU University Medical Centre. Subjects were assessed according to a clinical protocol, which involved history taking, physical and neurological examination, blood tests, MMSE (Folstein *et al*., 1975) neuropsychological work up (administration of a battery of neuropsychological tests), MRI of the brain according to a standard protocol and routine EEG. The final diagnosis was based upon a consensus meeting in which all the available clinical data and results of the ancillary investigations were considered. As reported in Stam *et al*. (2006), six patients used cholinesterase inhibitors, which was found to have no influence on functional connectivity. In the control and patient group both benzodiazepine and anti-depressive drug use was reported by one person. The study was approved by the Local Research Ethics Committee and all patients or their caregivers had given written informed consent. Since subjects were included years ago, medical files were checked again recently to verify initial diagnosis; no notable changes (besides disease progression) were discovered.

MEG recording

Magnetic fields were recorded while subjects were seated inside a magnetically shielded room (Vacuumschmelze GmbH, Hanau, Germany) using a 151-channel whole-head MEG system (CTF Systems Inc., Port Coquitlam, BC, Canada). Average distance between neighbouring sensors in this system was 3.1 cm. A third-order software gradient (Vrba *et al*., 1999) was used after online band-pass filtering between 0.25 and 125 Hz. Sample frequency was 625 Hz. For technical reasons two channels had to be omitted yielding 149 channels or sensors for analyses. Fields were measured during a no-task, eyes-closed condition. At the beginning and at the ending of the recording the head position relative to the coordinate system of the helmet was recorded by leading small alternating currents through three head position coils attached to the left and right pre-auricular points and the nasion on the subject's head. Head position changes during the recording up to ~1.5 cm were accepted. During the MEG recording, persons were instructed to sit comfortably, close their eyes and reduce eye movements, but remain awake as much as possible. During the recordings, the investigator and MEG technician checked the signal on-line for visual signs of drowsiness (e.g. slow eye movement activity) and observed the patient using a video monitor.

As a filtering process, offline frequency analysis is performed on the raw data, using a Fourier transformation. In the obtained frequency spectrum all frequencies outside the studied bands are set to zero, and using an inverse Fourier transformation the filtered signal is then obtained, with preservation of all phase information of the original data. For the subsequent off-line processing the recordings were converted to ASCII files and down-sampled to 312.5 Hz. For each subject care was taken to find and select exactly three artifact-free epochs of 4096 samples (13.083 s) by two of the investigators (BFJ and IM). MEG registrations were converted to datafiles with a coded filename before epoch selection, so the investigators were blind to the subjects' diagnosis during this process. Typical artifacts were due to (eye) movements, drowsiness or technical issues. Visual inspection and selection of epochs was realized with the DIGEEGXP software (CS). Epochs were band-pass filtered for the commonly used frequency bands: delta (0.5–4 Hz), theta (4–8 Hz), lower alpha (8–10 Hz), upper alpha (10–13 Hz), beta (13–30 Hz) and gamma (30–45 Hz), and all further analyses were performed for these bands separately.

Phase lag index

The PLI is a measure of the asymmetry of the distribution of phase differences between two signals. It reflects the consistency with which one signal is phase leading or lagging with respect to another signal (Stam *et al*., 2007*b*). The PLI performs at least as well as the synchronization likelihood (SL) (Montez *et al*., 2006) in detecting true changes in synchronization but it is much less affected by the influence of common sources. A more detailed explanation is offered in the Supplementary material to this article.

Beside a global, mean PLI calculation a more regional approach was used. For this analysis MEG sensors were grouped into five regions (frontal, temporal, central, parietal and occipital) for each hemisphere, and average PLI for all sensors within a region (local) or between two regions (long distance) were computed following the procedure described in Stam *et al*. (2006).

Graph analysis

In principle, networks can be represented by graphs, which are sets of vertices and corresponding sets of edges (Boccaletti *et al*., 2006; Stam and Reijneveld, 2007*c*). One may say that an edge or connection either exists or not but one may also assign a certain weight to an edge that reflects the importance or strength of the relation between two vertices. While the first one yields unweighted graphs in that edges have values of either 0 or 1, the latter produces so-called weighted graphs. To define the corresponding weights a matrix of correlations between signals recorded at different electrodes is generally suitable. We denote the matrix' coefficients as w_{ij}, i.e. they connect vertex i with vertex j and specified their values using the afore-explained PLI. That is we defined a network of 149 vertices (matching the 149 available MEG channels) and used the matrix of PLI values between all pairs of MEG channels as edge weights.

Graphs can be characterized by various measures. Two fundamental ones are the clustering coefficient, which denotes the likelihood that neighbours of a vertex will also be connected to each other, and the average path length, i.e. the average number of edges of the shortest path between pairs of vertices (Fig. 1).

Well ordered networks are strongly clustered and show large path lengths. In contrast, random networks are weakly clustered with small path lengths. Neither ordered nor random networks are good candidates for real networks like the human brain. Hence, Watts and Strogatz (1998) suggested a new type of networks, so-called small-world networks, which have both large clustering coefficients as well as small path lengths. Interestingly, these networks can be designed to be scale-free by having very short path lengths and a power law degree distribution (Barabási and Albert, 1999). Both small-world and scale-free networks are optimal in the sense that they allow efficient information processing with a minimal number of connections. By now it has been shown that many types of network ranging from metabolic and genetic to social are either small-world or scale-free (Amaral and Ottino, 2004; Boccaletti *et al*., 2006).

The clustering index C_i of a vertex i generally represents the likelihood that other vertices j that are connected to the vertex i will also be connected to each other. This notion can be adopted for use with weighted graphs in various ways (Boccaletti *et al*., 2006). Here we propose a simple definition, closely related to the proposal of Onnela *et al*. (2005), which only requires symmetry ($w_{ij} = w_{ji}$) and that $0 \leqslant w_{ij} \leqslant 1$ holds. Indeed, both conditions are readily fulfilled when using PLI as weight definition. The (weighted) clustering index of vertex i is then defined as

$$C_i = \frac{\sum_{k\neq i}\sum_{\substack{l\neq i\\ l\neq k}} w_{ik}w_{il}w_{kl}}{\sum_{k\neq i}\sum_{\substack{l\neq i\\ l\neq k}} w_{ik}w_{il}} \qquad (1)$$

Notice that in all sums in (1) terms with $k = i$, $l = i$ or $k = l$ are skipped. In the special case in which w_{ij} equals either 0 or 1, this definition is equivalent to the classical definition for unweighted graphs (Watts and Strogatz, 1998). For isolated vertices, i.e. vertices that do not have any connections, all weights w_{ij} vanish, and the clustering index is defined as $C_i = 0$ (Newman, 2003). The mean clustering coefficient of the entire network can be determined via (1) as

$$C_w = \frac{1}{N}\sum_{i=1}^{N} C_i \qquad (2)$$

Watts and Strogatz (1998) also defined the path length of unweighted graphs. We extend this definition to weighted graphs building on the approach of Latora and Marchiori (2001). In detail, we define the length of an edge as the inverse of the aforementioned edge weight, i.e. $L_{ij} = 1/w_{ij}$ if $w_{ij} \neq 0$, and $L_{ij} = +\infty$ if $w_{ij} = 0$; recall that w_{ij} is positive because we use the PLI as edge weight. The length of a weighted path between two vertices is then defined as the sum of the lengths of the edges of this path. The shortest path l_{ij} between two vertices i and j is the path between i and j with the shortest length. Analogously to definition (2) the average weighted path length of the entire graph is computed as

$$L_w = \frac{1}{(1/N(N-1))\sum_{i=1}^{N}\sum_{j\neq i}^{N}\left(1/L_{ij}\right)} \qquad (3)$$

Notice that instead of the arithmetic mean we here employed the harmonic mean (Newman, 2003), so that we can handle infinite path lengths between disconnected edges, i.e. $1/\infty \rightarrow 0$.

By definition, both values of C_w and L_w depend on edge weights and network structure but also on network size. In order to obtain measures that are independent of network size, the mean edge weight $\hat{C}_w = C_w/\langle C_w^{(\text{surrogate})}\rangle$ and the mean path length $\hat{L}_w = L_w/\langle L_w^{(\text{surrogate})}\rangle$ were computed, in which $\langle C_w^{(\text{surrogate})}\rangle$ and $\langle L_w^{(\text{surrogate})}\rangle$ denote weighted clustering coefficient and path length averaged over an ensemble of 50 surrogate random networks that were derived from the original networks by randomly reshuffling the edge weights. The steps

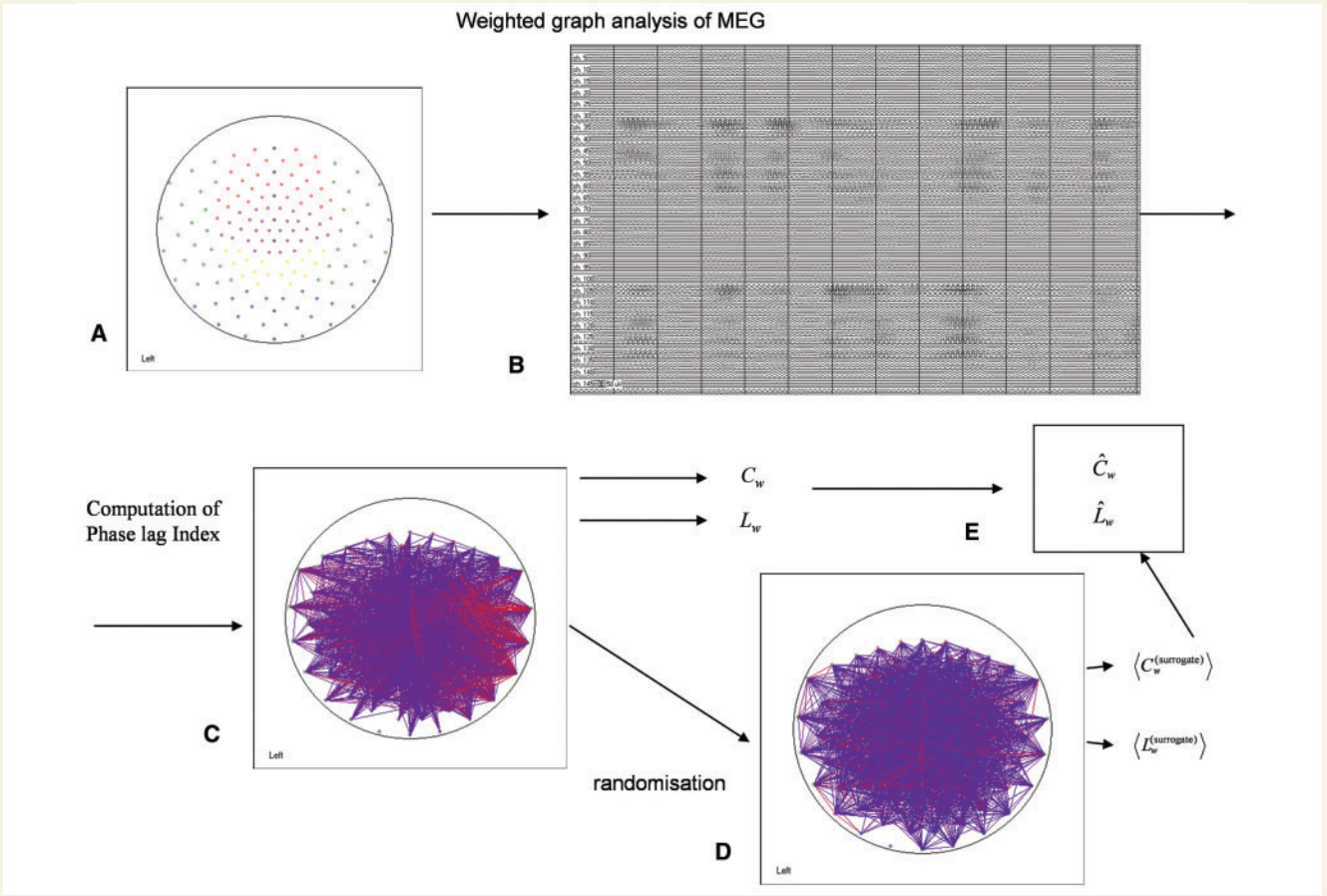

Fig. 2 Schematic illustration of the steps involved in weighted graph analysis of MEG recordings. At each of the MEG sensors, illustrated in (**A**), MEG signals are recorded. Epochs of MEG data are filtered, as shown in (**B**), and correlations between all pairs of channels are determined with the phase lag index. This results in a weighted graph, with the strength of the synchronization between pairs of sensors indicated in colour (blue low, red high PLI), as shown in (**C**). From each graph the weighted clustering coefficient C_w and the weighted path length L_w are computed. Also, from each graph, and ensemble of random graphs is generated by randomly shuffling the connection weights (**D**). The C_w and L_w of each of the random graphs is determined and the mean values for the ensemble, $\langle C_w^{(\text{surrogate})} \rangle$ and $\langle L_w^{(\text{surrogate})} \rangle$, are determined. Finally, the ratios $\hat{C}_w$ and $\hat{L}_w$ are computed (**E**).

involved in weighted graph analysis of the MEG data are illustrated schematically in Fig. 2.

Modelling network damage

To understand the general mechanisms underlying network changes in Alzheimer patients two models were compared, adopted from Albert and Barabási (2002). The first model (Random Failure) assumes that network changes are due to a random decrease in strength of edges. The second model (Targeted Attack) assumes that edges connecting high degree vertices ('hubs') will be more vulnerable to attack than edges connecting low degree vertices. The models were implemented by taking the PLI data of a control subject, selecting an edge at random, and then decrease its weight by a factor 2 with probability 1 (Random Failure model), or a probability that depended on the degree of both vertices connected by the edge (Targeted Attack model). This procedure was repeated until the average PLI of the network was decreased to the average PLI of the Alzheimer group (Figure 3). Data of all control subjects were treated in a similar way. This resulted in two new data sets, one for each model, which were subjected to the same graph analysis as the original control and Alzheimer data sets.

Statistical analysis

Statistical analysis was done with SPSS for MS-Windows (version 15). Group differences in respectively gender distribution and PLI and were tested with ANOVA (analysis of variance) and two-tailed *t*-tests for independent samples (not assuming equal variance). Since graph measures showed a non-Gaussian distribution, group differences were tested with Mann–Whitney U-tests for independent samples. The effect of and medication use on PLI and network measures was assessed using Kruskal–Wallis tests. Associations between cognitive status (MMSE) and PLI or network-derived measures were assessed with Spearman's bivariate correlation test. A significance level of $\alpha < 0.05$ was used.

Results

Subject characteristics

No effect of gender distribution in the groups on PLI values and network measures was found. In the Alzheimer's disease patient

group, six persons used cholinesterase inhibitors (rivastigmine or galantamine). However, use of this medication did not produce a significant effect on PLI or network measure outcomes. This was also the case for the use of other psychoactive drugs in both the patient and control group (see Patients and controls section).

Phase lag index

The average networks for Alzheimer's disease patients and controls computed with PLI in six different frequency bands are shown in Fig. 4.

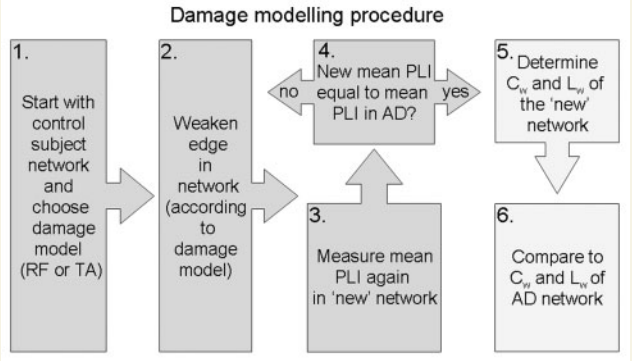

Fig. 3 Damage modelling procedure. The mean PLI of a control subject network is lowered by randomly weakening edges in the network, until it reaches the same value as in a Alzheimer's disease patient network. The effect of this damage is then examined by comparing the network characteristics of the damaged network to the Alzheimer's disease patient network characteristics. RF = Random Failure, TA = Targeted Attack, C_w = mean weighted clustering coefficient, L_w = mean weighted path length.

Visual inspection already suggested differences between the two groups, especially in the 8–10 Hz and 13–30 Hz bands. Group differences in mean PLI for each frequency band were tested with two-tailed *t*-tests for independent samples. The results are shown in Fig. 5.

The mean PLI was significantly lower in the Alzheimer's disease group in the 8–10 Hz band ($P = 0.022$) and in the 13–30 Hz band ($P = 0.036$). A non-significant trend in the same direction was found in the 10–13 Hz band ($P = 0.112$). No clear differences could be observed in other bands. By way of illustration, for the two frequency bands with a significant mean difference in PLI more detailed, regional results are shown in Fig. 6.

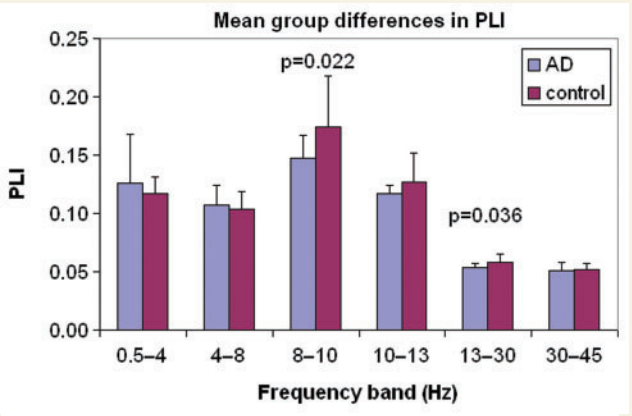

Fig. 5 Mean PLI averaged over all pairs of MEG sensors for Alzheimer's disease patients and controls in six frequency bands. Error bars are SDs. The mean PLI was significantly lower in Alzheimer's disease patients compared to controls in the lower alpha band (two-tailed *t*-test, $P < 0.022$) and the beta band (two-tailed *t*-test, $P = 0.036$).

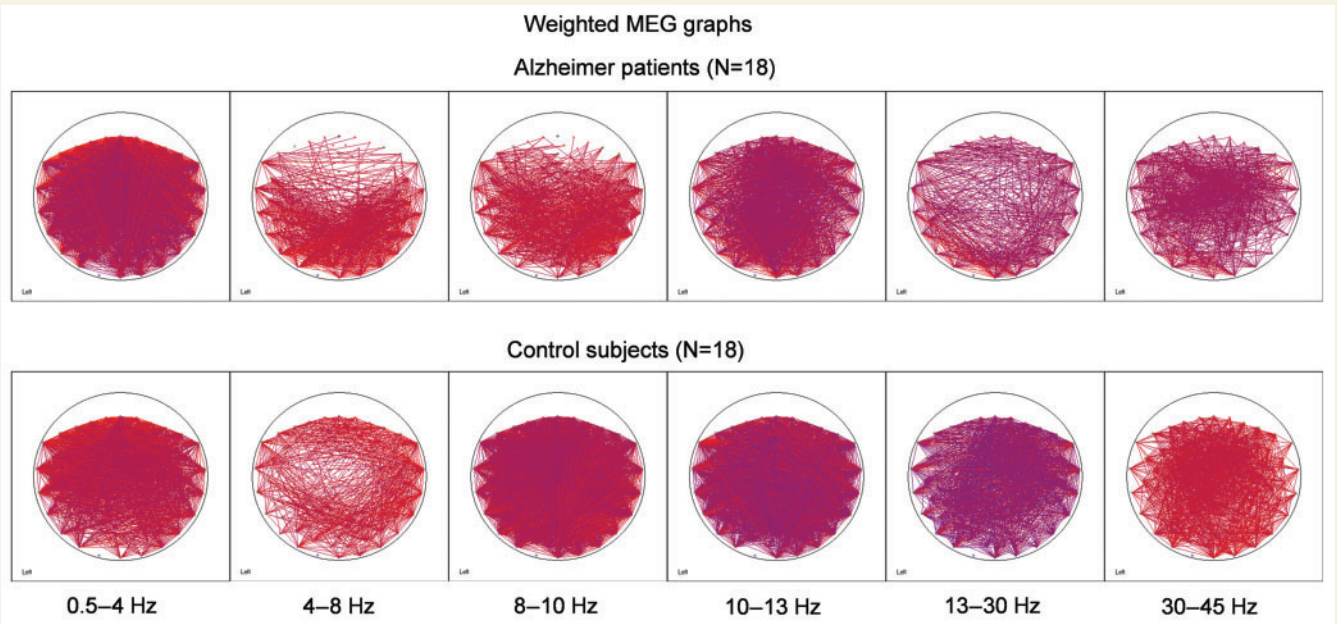

Fig. 4 Average weighted graphs of Alzheimer's disease patients and controls in six frequency bands. The value of the PLI for all individual pairs of MEG sensors is indicated in colour (blue: low PLI; red: high PLI).

For the 8–10 Hz band, Alzheimer's disease patients had significantly lower left fronto-parietal ($P = 0.026$), fronto-temporal ($P = 0.007$), parieto-occipital ($P = 0.025$) and temporo-occipital ($P = 0.009$) PLI. Local left frontal ($P = 0.034$), temporal ($P = 0.011$) and right parietal ($P = 0.021$) PLI were also decreased in the Alzheimer's disease group. For the 13–30 Hz band, Alzheimer's disease patients showed a decrease in interhemispheric frontal ($P = 0.032$), right fronto-parietal ($P = 0.041$) and local right ($P = 0.020$) and left ($P = 0.046$) frontal PLI.

Network analysis

Results of the weighted graph analysis are shown in Table 1.

The non-parametric Mann–Whitney U-test for independent samples revealed that C_w was lower in Alzheimer's disease subjects in the 8–10 Hz band ($U = 89.5$; $P = 0.022$), but not in the 13–30 Hz band ($U = 107.0$; $P = 0.081$). L_w was higher in Alzheimer's disease subjects in the 8–10 Hz band ($U = 82.0$; $P = 0.011$). In the 8–10 Hz band Alzheimer's disease patients had a lower $\hat{C}_w$ ($U = 76.0$; $P = 0.006$) and a lower $\hat{L}_w$ ($U = 86.0$; $P = 0.016$).

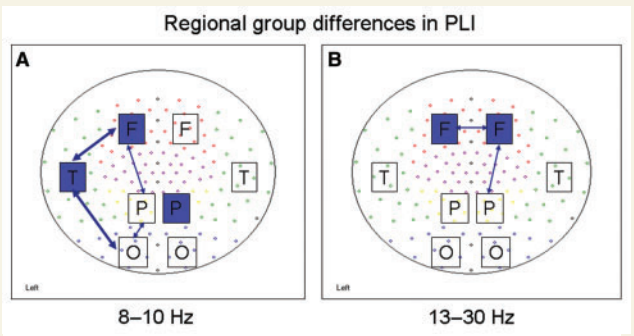

Fig. 6 Schematic illustration of significant differences in long distance (indicated by arrows) and short distance (indicated by filled squares) PLI in the 8–10 Hz and 13–30 Hz band. Alzheimer's disease patients had lower left sided fronto-temporal, fronto-parietal, temporo-occipital and parieto-occipital PLI in the 8–10 Hz band. Local left frontal and temporal, and right parietal PLI were also decreased in Alzheimer's disease patients (**A**). For the 13–30 Hz band, Alzheimer's disease patients had lower inter hemispheric frontal, right fronto-parietal and bilateral frontal PLI (**B**).

Modelling of network changes

Modelling with the Random Failure and the Targeted Attack model was applied to the data of the 8–10 Hz band since this band showed the most consistent differences in graph measures between the two groups. The average PLI graphs for Alzheimer's disease patients, controls and both models are shown in Fig. 7. On visual inspection, both models look quite similar to the average network in the Alzheimer's disease group. Please note that, by definition, the average PLI of both models is the same as the average PLI of the Alzheimer's disease data.

Further analysis of the model data compared with the real data is shown in Fig. 8. For the Random Failure model the $\hat{C}_w$ was not different from the control data, and significantly higher than $\hat{C}_w$ of the Alzheimer's disease group (Mann–Whitney U-test, $U = 76.5$; $P = 0.007$). In contrast, $\hat{C}_w$ of the Targeted Attack model was not significantly different from the Alzheimer's disease group, but significantly lower than $\hat{C}_w$ of the control group ($U = 87.0$; $P = 0.018$). The weighted path length $\hat{L}_w$ showed a decreasing trend going from controls to Random Failure, Targeted Failure and controls (Fig. 8, right panel). $\hat{L}_w$ of both models did not differ significantly from control data.

Correlation with MMSE

No significant correlations between MMSE and PLI or network measures were found in the Alzheimer's disease patient group (Fig. 9). When correlation with MMSE was analysed for all subjects (Alzheimer's disease and control) put together in one group, we found significant effects between MMSE and mean PLI in the beta band (Spearman's $r = 0.570$, $P = 0.001$) and between MMSE and $\hat{C}_w$ in the lower alpha band (Spearman's $r = 0.475$, $P = 0.008$).

Table 1 Results of weighted graph analysis for Alzheimer's disease patients and controls in six frequency bands

	C_w		L_w		$\hat{C}_w$		$\hat{L}_w$	
	Alzheimer's disease	Control	Alzheimer's disease	Control	Alzheimer's disease	Control	Alzheimer's disease	Control
0.5–4 Hz	0.12 (0.10–0.32)	0.12 (0.10–0.17)	4.05 (1.69–4.40)	3.92 (2.89–4.59)	1.04 (1.03–1.12)	1.04 (1.02–1.11)	1.09 (1.06–1.33)	1.08 (1.05–1.34)
4–8 Hz	0.11 (0.09–0.20)	0.10 (0.09–0.15)	4.23 (2.48–4.99)	4.44 (3.22–5.01)	1.05 (1.03–1.17)	1.04 (1.03–1.13)	1.14 (1.04–1.41)	1.15 (1.05–1.43)
8–10 Hz	**0.15 (0.12–0.21)**	**0.17 (0.13–0.29)**	**3.27 (2.25–3.76)**	**2.69 (1.80–3.73)**	**1.04 (1.02–1.12)**	**1.07 (1.04–1.13)**	**1.08 (1.05–1.32)**	**1.19 (1.07–1.30)**
10–13 Hz	0.12 (0.11–0.14)	0.13 (0.11–0.22)	3.83 (3.28–4.36)	3.72 (2.36–4.30)	1.04 (1.03–1.10)	1.04 (1.03–1.21)	1.10 (1.05–1.35)	1.12 (1.04–1.45)
13–30 Hz	0.06 (0.05–0.06)	0.06 (0.05–0.08)	7.97 (6.44–9.24)	7.61 (5.18–9.35)	1.04 (1.02–1.07)	1.04 (1.03–1.16)	1.11 (1.05–1.50)	1.12 (1.04–1.50)
30–45 Hz	0.05 (0.05–0.09)	0.05 (0.05–0.08)	8.70 (5.17–9.07)	8.54 (6.06–9.14)	1.02 (1.02–1.07)	1.02 (1.02–1.07)	1.09 (1.06–1.33)	1.04 (1.02–1.30)

Values are medians, with range printed between parentheses. C_w = mean weighted clustering coefficient; L_w = mean weighted path length; $\hat{C}_w$ = mean normalized average weighted clustering coefficient (see Materials and Methods section), $\hat{L}_w$ = mean normalized average weighted path length. Significant differences between Alzheimer's disease and controls with non-parametric testing (Mann–Whitney U-test, $P < 0.05$) are given in bold.

Discussion

The present study showed that resting-state functional connectivity of MEG is decreased in Alzheimer's disease patients in the lower alpha and beta bands using a recently developed measure, the PLI that appears invariant against volume conduction. This finding supports the concept of Alzheimer's disease as a disconnection syndrome. Moreover, changes in functional connectivity in Alzheimer's disease patients did not involve all brain regions to the same extent, suggesting a heterogeneous disruption of overall network structure. This idea was confirmed by graph analysis of the functional connectivity data, which revealed lower normalized clustering coefficients and path lengths in the Alzheimer's disease group in the lower alpha band. This type of change suggests that brain networks in Alzheimer's disease patients are closer to random networks than those of non-demented control subjects. The modelling results suggest that this change was brought about by a preferential decrease of connections between high degree nodes ('hubs'), rather than a non-specific decrease of connection strength.

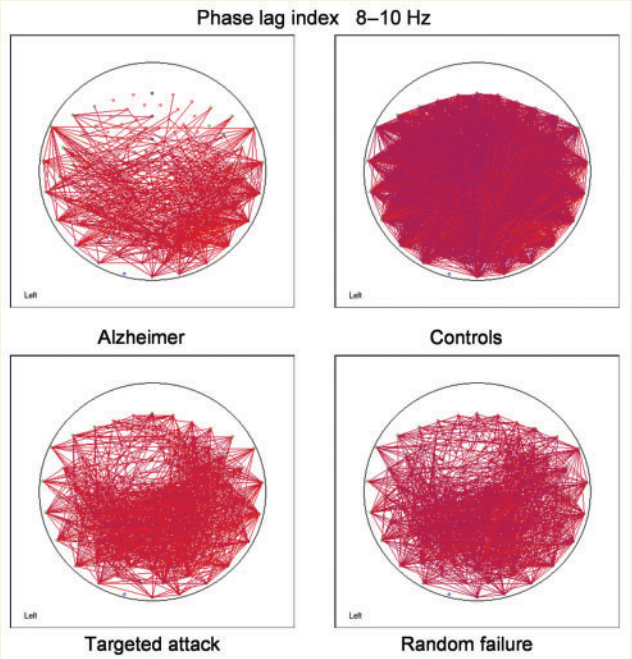

Fig. 7 Comparison of real and modelled networks in the 8–10 Hz band. Top left: average PLI for the Alzheimer patients. Top right: average PLI for the control subjects. Bottom left: average PLI after application of the 'Targeted Attack' model to control data. Bottom right: average PLI after application of the 'Random Failure' model to control data.

Volume conduction

A decrease of resting state functional connectivity in Alzheimer's disease patients in the alpha and often also in the beta band has been reported in many EEG and MEG studies (Leuchter *et al.*, 1992; Besthorn *et al.*, 1994; Dunkin *et al.*, 1994; Jelic *et al.*, 1996; Locatelli *et al.*, 1998; Knott *et al.*, 2000; Stevens *et al.*, 2001; Adler *et al.*, 2003; Hogan *et al.*, 2003; Jiang 2005; Koenig *et al.*, 2005; Pogarell *et al.*, 2005). However, a major point of criticism is that such studies were done on the raw EEG and MEG time series. It is well known that estimates of statistical interdependencies in EEG and MEG may be biased by the effects of volume conduction and, in the case of EEG, by the influence of the reference electrode (Nunez *et al.*, 1997; Guevara *et al.*, 2005). More specifically, nearby EEG

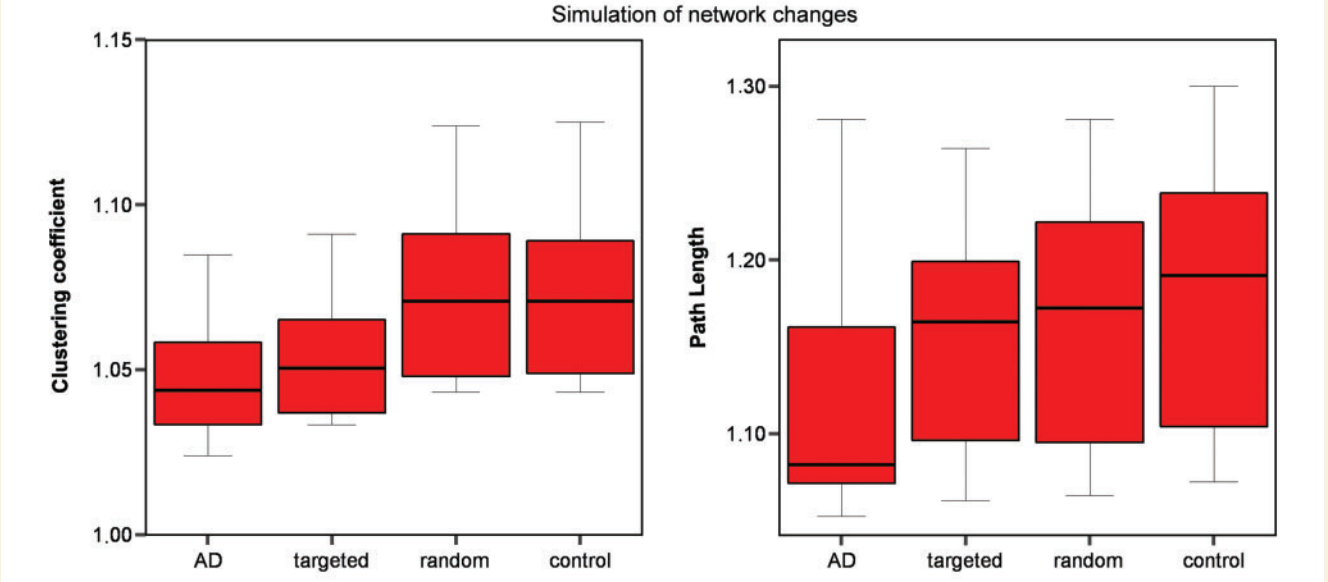

Fig. 8 Comparison of normalized weighted clustering coefficient (left panel) and path length (right panel) for Alzheimer patients, Targeted Attack model, Random Failure model and controls in the 8–10 Hz band. Box plots show median, interquartile range and extremes.

electrodes or MEG sensors are likely to pick up activity of the same source, and thereby to display spuriously high correlations between their time series. This problem can be solved to a large degree by acknowledging that spurious couplings due to volume conduction or active reference electrodes cannot give rise to phase delays between channels. The PLI is only sensitive to phase synchronization between two channels when one is consistently leading or lagging in phase with respect to the other. That is, with PLI any coupling with a phase difference which centres around 0 mod π are discounted. Put differently, our finding of a significant decrease of PLI in the lower alpha and the beta band cannot be explained by volume conduction but strongly supports the idea that resting-state functional connectivity is decreased in Alzheimer's disease. Since the PLI results are largely in line with the previous studies we can conclude that the influence of volume conduction and reference electrode in these studies may have been smaller than has sometimes been suggested. However, a detailed comparison of our study with a previous study, in which the same data were analysed with several linear and nonlinear measures, does display a few differences (Stam *et al*., 2006). For example, if we compare Fig. 6 of the present study with Figs 3, 4 and 7 of Stam *et al*. (2006), one finds that the PLI in the beta band only showed decreases in the Alzheimer's disease group, whereas coherence and SL also showed centro-parietal increases. A possible explanation could be that the increases in connectivity reported for SL and coherence might be influenced by volume conduction, while the decreases seems to be confirmed by the PLI and may reflect true loss of connectivity, but this should be subject to further study.

Resting state

Functional connectivity can be determined in relation to tasks as well as during a resting state. More recently there has been a growing interest in resting state functional connectivity because it appears that in particular memory-related brain networks are consistently activated during this state (Gusnard and Raichle, 2001; Laufs *et al*., 2003; Damoiseaux *et al*., 2006). Moreover, resting state functional connectivity has a strong genetic component, and shows characteristic changes in various psychiatric and neurological disorders (Posthuma *et al*., 2005; Stam, 2005, 2006).

Network analysis

In the present study C_w was decreased in the lower alpha and beta band and L_w was increased in the lower alpha band in the Alzheimer's disease group. It should be stressed that these changes in C_w and L_w are likely to be influenced by changes in the PLI. A lower mean level of PLI will decrease the estimate of C_w, irrespective of changes in network structure. Similarly, a lower PLI will give rise to longer weighted path lengths. These results should be compared to Fig. 5 in Stam *et al*. (2007*a*). Here C_w and L_w were compared between controls and Alzheimer's disease patients for the same threshold, showing a non-significant trend to a lower C_w and a significant increase of L_w in the Alzheimer's disease group. By using the same threshold for both groups, differences in mean PLI could have influenced the results. Thus changes in C_w and L_w in both studies are consistent, but cannot be taken as 'pure' measures of changes in network

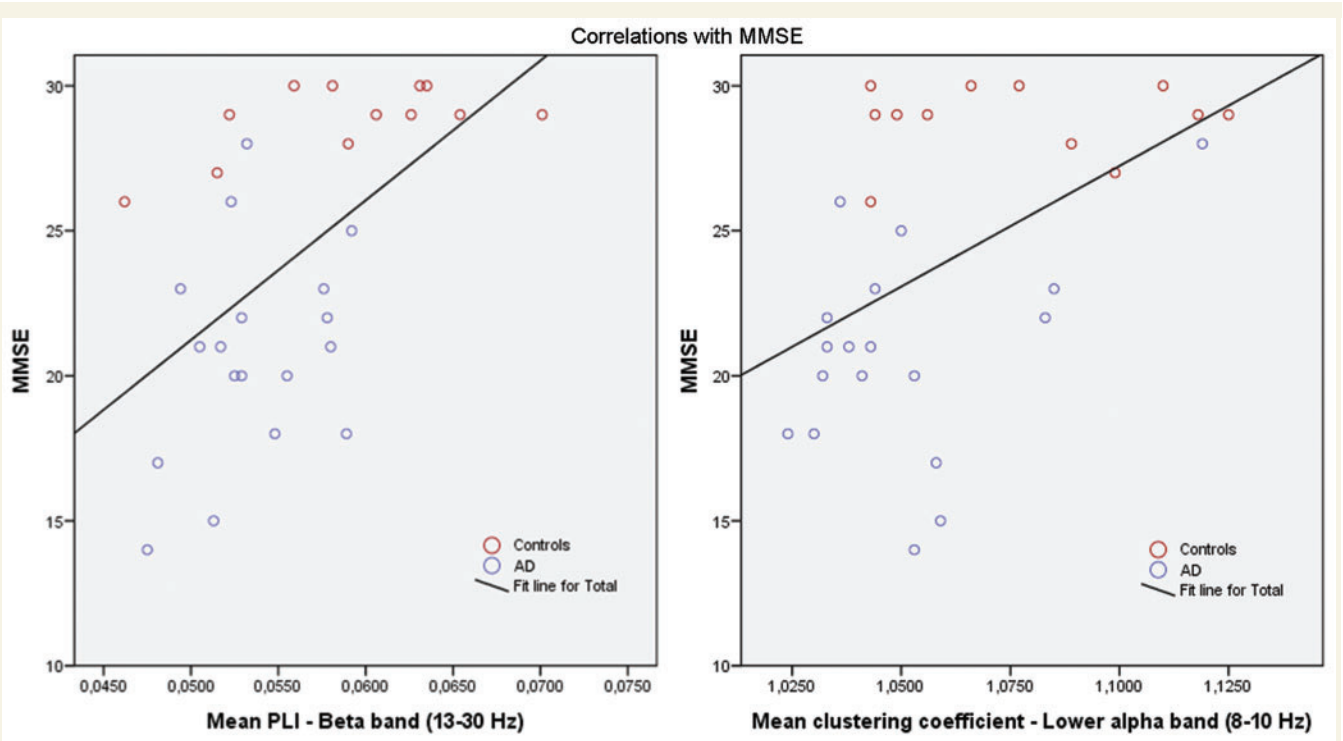

Fig. 9 In the left panel the correlation of mean PLI in the lower alpha band and MMSE is shown (Spearman's $r = 0.570$, $P = 0.001$), in the right panel the correlation of the mean clustering coefficient with MMSE in the beta band (Spearman's $r = 0.475$, $P = 0.008$). Alzheimer's disease and controls group were combined for this analysis.

structure as they are likely to be influenced by the lower mean level of connectivity in the Alzheimer's disease group.

In contrast, the normalized coefficients $\hat{C}_w$ and $\hat{L}_w$ are corrected for differences in mean PLI between subjects, since each network is compared to its own random counterpart. The most important result is thus the decrease of $\hat{C}_w$ and $\hat{L}_w$ in the Alzheimer's disease group in the lower alpha band. Within the framework of the Watts and Strogatz model this suggests that network architecture in Alzheimer's disease patients is significantly closer to that of random networks. However, $\hat{C}_w$ was very close to one in both groups, and much lower than reported in other studies, where $\hat{C}_w$ was usually around two (Stam, 2004; Salvador *et al*., 2005; Achard *et al*., 2006; Bassett *et al*., 2006; Stam *et al*., 2007*a*). It is possible that correlations between nearby sensors due to volume conduction could have produced spuriously high estimates of C_w in previous EEG and MEG studies.

Damage modelling

Modelling was used to investigate whether the observed network changes in Alzheimer's disease in the 8–10 Hz band could be explained by a general mechanism. In the literature on complex networks generally two types of network damage are considered: Random Failure, where edges and/or vertices are lost randomly, and Targeted Attack, where damage mainly affects high degree, critical vertices and/or edges (section 3 in Boccaletti *et al*., 2006, for a more practical application see Kaiser *et al*., 2007). In our study the Targeted Attack model performed better than the random error model in explaining the network changes in Alzheimer's disease, in particular with respect to the clustering coefficient (Fig. 7). While both models lowered the mean PLI to the level observed in the Alzheimer's disease group, only the Targeted Attack model produced a clustering coefficient as low as in the patients, whereas the Random Failure model did not change the clustering coefficient at all. These results suggest that the disease process in Alzheimer's disease may specifically affect association fibres connecting brain areas that are highly connected to the rest of the brain, that is: higher order association areas. The distribution of amyloid plaques in Alzheimer's disease is in agreement with this suggestion (Nordberg, 2007).

Several studies have investigated the nature of network changes in different types of brain pathology. In the case of brain tumours, schizophrenia and interictal recordings of patients with epilepsy pathological networks were characterized by a smaller C_w and a smaller L_w (Bartolomei *et al*., 2006; Micheloyannis *et al*., 2006; Ponten *et al*., 2007; Rubinov *et al*., 2007). Considering the model of Watts and Strogatz, where the edges of a fully ordered network with degree K (number of edges per vertex) are rewired randomly with a certain probability P, a lower C_w and L_w would correspond with a higher value of the rewiring probability, and a more random network. The findings in the Alzheimer's disease group in the present study seem to fit in the same scheme: decrease of both C_w and L_w, and a more random network in the patient group. Moreover, the values were close to (although significantly different from) 1, which indicates that the difference between real and random networks was very small. The one finding that does not fit in this pattern is the increase in beta band path length for Alzheimer's disease patients reported in the previous pilot study (Stam *et al*., 2007*a*). This result was obtained only for some values of degree K, with K identical for both groups (Fig. 5 in Stam *et al*., 2007*a*). One explanation could be that in the EEG pilot study disconnected points (which occur already for values of $K = 3$) were excluded from the computation of the path length, whereas in the present study they were included (see formula in Materials and methods section). This is an essential difference, excluding or including disconnected points may decrease or increase the estimated path length considerably. The lower alpha band, which was the only band to show clear changes in normalized clustering coefficient and path length in the current MEG study, was not investigated in the EEG study. Therefore, the evidence in favour of more random network topology in Alzheimer's disease seems to be stronger, and in line with changes in other disorders. To be able to find a disease-specific 'network change profile' probably requires further exploration of this network approach and its relation to clinical features of Alzheimer's disease. Possibly 'network randomization' may be a final common pathway for different types of brain damage, resulting from loss of neurons and connections as well a random outgrowth of new connections. A related concept of increased entropy relating to ageing and Alzheimer's disease has recently been formulated by Drachmann: 'Increasing entropy, manifest through a complex network of interacting age related changes, is seen as the fundamental driving cause of neural and cognitive decline in the elderly, as well as the overriding etiologic principle in further transition to sporadic Alzheimer's disease' (Drachmann, 2006). It would be of considerable interest to study how different types of treatment will interfere with this process of network randomization, and how the network parameters relate to disease severity and cognitive performance.

Supplementary material

Supplementary material is available at *Brain* online.

Acknowledgement

The authors thank Mrs Els van Deventer for continuing support in retrieving relevant literature.

Funding

Alzheimer Nederland; Dutch Science Foundation (NWO, grant #452-04-344).

References

Achard S, Salvador R, Whitcher B, Suckling J, Bullmore E. A resilient, low-frequency, small-world human brain functional network with highly connected association cortical hubs. J Neurosci 2006; 26: 63–72.

Adler G, Brassen S, Jajcevic A. EEG coherence in Alzheimer's dementia. J Neural Transm 2003; 110: 1051–8.

Aertsen AMHJ, Gerstein GL, Habib MK, Palm G. Dynamics of neuronal firing correlation: modulation of 'effective connectivity'. J Neurophysiol 1989; 61: 900–17.

Albert R, Barabási AL. Statistical mechanics of complex networks. Rev Mod Physics 2002; 74: 47–97.

Amaral LAN, Ottino JM. Complex networks. Augmenting the framework for the study of complex systems. Eur Phys J B 2004; 38: 147–62.

Amor F, Rudrauf D, Navarro V, N'diaye K, Garnero L, Martinerie J, et al. Imaging brain synchrony at high spatio-temporal resolution: application to MEG signals during absence seizures. Signal Process 2005; 85: 2101–11.

Babiloni C, Ferri F, Moretti DV, Strambi A, Binetti G, Dal Forno G, et al. Abnormal fronto-parieto coupling of brain rhythms in mild Alzheimer's disease: a multicentric EEG study. Eur J Neurosci 2004; 19: 1–9.

Barabasi AL, Albert R. Emergence of scaling in random networks. Science 1999; 286: 509–12.

Bartolomei F, Bosma I, Klein M, Baayen JC, Reijneveld JC, Postma TJ, et al. Disturbed functional connectivity in brain tumour patients: evaluation by graph analysis of synchronization matrices. Clin Neurophysiol 2006; 117: 2039–49.

Bassett DS, Bullmore E. Small-world brain networks. Neuroscientist 2006; 12: 512–23.

Basset DS, Meyer-Linderberg A, Achard S, Duke Th, Bullmore E. Adaptive reconfiguration of fractal small-world human brain functional networks. PNAS 2006; 103: 19518–23.

Berendse HW, Verbunt JPA, Scheltens P, van Dijk BW, Jonkman EJ. Magnetoencephalographic analysis of cortical activity in Alzheimer's disease. A pilot study. Clin Neurophysiol 2000; 111: 604–12.

Besthorn C, Forstl H, Geiger-Kabisch C, Sattel H, Gasser T, Schreiter-Gasser U. EEG coherence in Alzheimer disease. Electroenceph Clin Neurophysiol 1994; 90: 242–5.

Boccaletti S, Latora V, Moreno Y, Chavez M, Hwang D-U. Complex networks: structure and dynamics. Physics Reports 2006; 424: 175–308.

Damoiseaux JS, Rombouts SARB, Barkhof F, Scheltens P, Stam C, Smith SM, et al. Consistent resting-state networks across healthy subjects. PNAS 2006; 103: 13848–53.

David O, Garnero L, Cosmelli D, Varela FJ. Estimation of neural dynamics from MEG/EEG cortical current density maps: application to the reconstruction of large-scale cortical synchrony. IEEE Trans Biomed Eng 2002; 49: 975–87.

Delbeuck X, Van der Linder M, Colette F. Alzheimer's disease as a disconnection syndrome? Neuropyschol Rev 2003; 13: 79–92.

Drachman DA. Aging of the brain, entropy, and Alzheimer disease. Neurology 2006; 24; 67: 1340–52.

Dunkin JJ, Leuchter AF, Newton TF, Cook IA. Reduced EEG coherence in dementia: state or trait marker? Biol Psychiatr 1994; 35: 870–79.

Fingelkurts AA, Fingelkurts AA, Kahkonen S. Functional connectivity in the brain – is it a elusive concept? Neurosci Biobehav Rev 2005; 28: 827–36.

Folstein MF, Folstein SE, McHugh PR. 'Mini-mental state'. A practical method for grading the cognitive state of patients for the clinician. J Psychiatr Res 1975; 12: 189–98.

Friston KJ. Brain function, nonlinear coupling, and neuronal transients. The Neuroscientist 2001; 7: 406–18.

Friston KJ. Functional integration and inference in the brain. Progress Neurobiol 2002; 68: 113–43.

Gross J, Kujala J, Hamalainen M, Timmermann L, Schnitzler A, Salmelin R. Dynamic imaging of coherent sources: studying neural interactions in the human brain. PNAS 2001; 98: 694–9.

Guevara R, Velazguez JLP, Nenadovic V, Wennberg R, Senjanovic G, Dominguez LG. Phase synchronization measurements using electroencephalographic recordings. What can we really say about neuronal synchrony? Neuroinformatics 2005; 3: 301–14.

Gusnard DA, Raichle ME. Searching for a baseline: functional imaging and the resting brain. Nature Rev Neurosci 2001; 2: 685–94.

Hadjipapas A, Hillebrand A, Holliday IE, Singh K, Barnes G. Assessing interactions of linear and nonlinear neuronal sources using MEG beamformers: a proof of concept. Clin Neurophysiol 2005; 116: 1300–13.

He Y, Chen ZJ, Evans AC. Small-world anatomical networks in the human brain revealed by cortical thickness form MRI. Cerebral Cortex 2007; 17: 2407–19.

Hilgetag CC, Burns GAPC, O'Neill MAO, Scannell JW, Young MP. Anatomical connectivity defines the organization of clusters of cortical areas in the macaque monkey and the cat. Philosophic Trans Biol Sci 2000; 355: 91–110.

Hogan MJ, Swanwick GRJ, Kaiser J, Rowan M, Lawlor B. Memory-related EEG power and coherence reductions in mild Alzheimer's disease. Int J Psychophysiol 2003; 49: 147–63.

Iturria-Medina Y, Sotero RC, Canales-Rodriguez EJ, eman-Gomez Y, Melie-Garcia L. Studying the human brain anatomical network via diffusion-weighted MRI and Graph Theory. Neuroimage 2008; 40: 1064–76.

Jelic V, Shigeta M, Julin P, Almkvist O, Winblad B, Wahlung WO. Quantitative electroencephalography power and coherence in Alzheimer's disease and mild cognitive impairment. Dementia 1996; 7: 314–23.

Jeong J, Gore JC, Peterson BS. Mutual information analysis of the EEG in patients with Alzheimer's disease. Clin Neurophysiol 2001; 112: 827–35.

Jiang ZY. Abnormal cortical functional connections in Alzheimer's disease: analysis of inter- and intra-hemispheric EEG coherence. J Zheniang Univ Sci B 2005; 6: 259–64.

Kaiser M, Martin R, Andras P, Young MP. Simulation of robustness against lesions of cortical networks. Eur J Neurosci 2007; 25: 3185–92.

Koenig T, Prichep L, Dierks T, Hubl D, Wahlund LO, John ER, et al. Decreased EEG synchronization in Alzheimer's disease and mild cognitive impairment. Neurobiol Aging 2005; 26: 165–71.

Knott V, Mohr E, Mahoney C, Ilivitsky V. Electroencephalographic coherence in Alzheimer's disease: comparisons with a control group and population norms. J Geriatr Psychiatry Neurol 2000; 13: 1–8.

Latora V, Marchiori M. Efficient behavior of small-world networks. Phys Rev Lett 2001; 87: 198701.

Laufs H, Krakow K, Sterzer P, Eger E, Beyerle A, Salek-Haddadi A, et al. Electroencephalographic signatures of attentional and cognitive default modes in spontaneous brain acitivity fluctuations at rest. PNAS 2003; 100: 11053–8.

Lee L, Harrison LM, Mechelli A. A report of the functional connectivity workshop, Dusseldorf 2002. NeuroImage 2003; 19: 457–65.

Lehmann D, Faber PL, Gianotti LRR, Kochi K, Pascual-Marqui RD. Coherence and phase locking in the scalp EEG and between LORETA model sources, and microstates as putative mechanisms of brain temporo-spatial functional organization. J Physiol 2006; 99: 29–36.

Leuchter AF, Newton TF, Cook AA, Walter DO. Changes in brain functional connectivity in Alzheimer-type and multi-infarct dementia. Brain 1992; 115: 1543–61.

Le van Quyen M. Disentangling the dynamic core: a research program for a neurodynamics at the large scale. Biol Res 2003; 36: 67–88.

Locatelli T, Cursi M, Liberati D, Francheschi M, Comi G. EEG coherence in Alzheimer's disease. Electroenceph Clin Neurophysiol 1998; 106: 229–37.

McKhann G, Drachman D, Folstein M, Katzman R, Price D, Stadlan EM. Clinical diagnosis of Alzheimer's disease: report of the NINCDS-ADRDA Work Group under the auspices of Department of Health and Human Services Task Force on Alzheimer's Disease. Neurology 1984; 34: 939–44.

Micheloyannis S, Pachou E, Stam CJ, Breakspear M, Bitsios P, Vourkas M, et al. Small-world networks and disturbed functional connectivity in schizophrenia. Schizophr Res 2006; 87: 60–6.

Montez T, Linkenkaer-Hansen K, van Dijk BW, Stam CJ. Synchronization likelihood with explicit time-frequency priors. Neuroimage 2006; 33: 1117–25.

Newman ME. Properties of highly clustered networks. Phys Rev E Stat Nonlin Soft Matter Phys 2003; 68 (2 Pt 2): 026121.

Nordberg A. Amyloid imaging in Alzheimer's disease. Curr Opin Neurol 2007; 20: 398–402.

Nolte G, Wheaton OBL, Mari Z, Vorbach S, Hallett M. Identifying true brain interaction from Eeg data using the imaginary part of coherency. Clin Neurophysiol 2004; 115: 2292–307.

Nunez PL, Srinivasan R, Westdorp AF, Wijesinghe RS, Tucker DM, Silberstein RB, et al. EEG coherency I: statistics, reference electrode, volume conduction, Laplacians, cortical imaging, and interpretation at multiple scales. Electroenceph Clin Neurophysiol 1997; 103: 499–515.

Onnela J-P, Saramaki J, Kertesz J, Kaski K. Intensity and coherence of motifs in weighted complex networks. Phys Rev E 2005; 71: 065103(R).

Osipova D, Ahveninen J, Kaakkola S, Jääskeläinen IP, Huttunen J, Pekkonen E. Effects of scopolamine on MEG spectral power and coherence in elderly subjects. Clin Neurophysiol 2003; 114: 1902–7.

Pijnenburg YAL, van de Made Y, van Cappellen van Walsum AM, Knol DL, Scheltens Ph, Stam CJ. EEG synchronization likelihood in mild cognitive impairment and Alzheimer's disease during a working memory task. Clin Neurophysiol 2004; 115: 1332–9.

Pikovsky A, Rosenblum M, Kurths J. Synchronization. A Universal Concept in Nonlinear Sciences. Cambridge Nonlinear Science Series 12. Cambridge: Cambridge University Press; 2001.

Pogarell O, Teipel SJ, Juckel G, Gootjes L, Moller T, Burger K, et al. EEG coherence reflects regional corpus callosum area in Alzheimer's disease. J Neurol Neurosurg Psychiatr 2005; 76: 109–11.

Ponten SC, Bartolomei F, Stam CJ. Small-world networks and epilepsy: graph theoretical analysis of intracerebrally recorded mesial lobe seizures. Clin Neurophysiol 2007; 118: 918–27.

Posthuma D, de Geus EJC, Mulder EJCM, Smit DJA, Boomsma DI, Stam CJ. Genetic components of functional connectivity in the brain: the heritability of synchronization likelihood. Human Brain Mapp 2005; 26: 191–8.

Rubinov M, Knock SA, Stam CJ, Micheloyannis S, Harris AW, Williams LM, et al. Small-world properties of nonlinear brain activity in schizophrenia. Hum Brain Mapp 2007; December 10 (Epub ahead of print).

Salvador R, Suckling J, Coleman MR, Pickard JD, Menon D, Bullmore E. Neurophysiological architecture of functional magnetic resonance images of human brain. Cereb Cortex 2005; 15: 1332–42.

Srinivasan R, Winter WR, Ding J, Nunez PL. EEG and MEG coherence: measures of functional connectivity at distinct spatial scales of neocortical dynamics. J Neurosci Methods 2007; 166: 41–52.

Smit DJ, Stam CJ, Posthuma D, Boomsma DI, de Geus EJ. Heritability of 'small-world' networks in the brain: a graph theoretical analysis of resting-state EEG functional connectivity. Hum Brain Mapp 2007; December 6 (Epub ahead of print).

Stam CJ. Functional connectivity patterns of human magnetoencephalographic recordings: a 'small-world' network? Neurosci Lett 2004; 355: 25–8.

Stam CJ. Nonlinear dynamical analysis of EEG and MEG: review of an emerging field. Clin Neurophysiol 2005; 116: 2266–301.

Stam CJ. Nonlinear brain dynamics. New York: Nova Science Publishers; 2006.

Stam CJ, van Cappellen van Walsum AM, Pijnenburg YAL, Berendse HW, de Munck JC, Scheltens Ph, et al. Generalized synchronization of MEG recordings in Alzheimer's disease: evidence for involvement of the gamma band. J Clin Neurophysiol 2002; 19: 562–74.

Stam CJ, Jones BF, Manshanden I, van Cappellen van Walsum AM, Montez T, Verbunt JPA, et al. Magnetoencephalographic evaluation of resting-state functional connectivity in Alzheimer's disease. Neuroimage 2006; 32: 1335–44.

Stam CJ, Jones BF, Nolte G, Breakspear M, Scheltens P. Small-world networks and functional connectivity in Alzheimer's disease. Cereb Cortex 2007a; 17: 92–9.

Stam CJ, Nolte G, Daffertshofer A. Phase lag index: Assessment of functional connectivity from multi channel EEG and MEG with diminished bias from common sources. Hum Brain Mapp 2007b; 28: 1178–93.

Stam CJ, Reijneveld JC. Graph theoretical analysis of complex networks in the brain. Nonlinear Biomed Phys 2007c; 1: 3.

Stevens A, Kircher T, Nickola M, Bartels M, Rosellen N, Wormstall H. Dynamic regulation of EEG power and coherence is lost early and globally in probable DAT. Eur Arch Psychiatry Clin Neurosci 2001; 251: 199–204.

Supekar K, Menon V, Rubin D, Musen M, Greicius MD. Network analysis of intrinsic functional brain connectivity in Alzheimer's disease. PLoS Comput Biol 2008; 4: e1000100.

Tass PA, Fieseler T, Dammers J, Dolan K, Morosan P, Majtanik M, et al. Synchronization tomography: a method for three-dimensional localization of phase synchronized neuronal populations in the human brain using magnetoencephalography. Phys Rev Lett 2003; 90: 088101.

van der Flier WM, Scheltens P. Epidemiology and risk factors of dementia. J Neurol Neurosurg Psychiatr 2005; 76 (Suppl 5): v2–7.

Varela F, Lachaux J-P, Rodriguez E, Martinerie J. The brainweb: phase synchronization and large-scale integration. Nature Rev Neurosci 2001; 2: 229–39.

Vrba J, Anderson G, Betts K, Burbank MB, Cheung T, Cheyne D, et al. 151-Channel whole-cortex MEG system for seated or supine positions. In: Yoshimoto T, Kotani M, Kuriki S, Karibe H, Nakasato N, editors. Recent advances in biomagnetism. Sendai, Japan: Tohoku University Press; 1999. p. 93–6.

Watts DJ, Strogatz SH. Collective dynamics of 'small-world' networks. Nature 1998; 393: 440–2.